Nonreciprocal transmission of magnetoacoustic waves in compensated synthetic antiferromagnets

M. Küß,[1,2,*] M. Hassan,[2] Y. Kunz,[3] A. Hörner,[1] M. Weiler,[3] and M. Albrecht[2]

[1]*Experimental Physics I, Institute of Physics, University of Augsburg, 86135 Augsburg, Germany*

[2]*Experimental Physics IV, Institute of Physics, University of Augsburg, 86135 Augsburg, Germany*

[3]*Fachbereich Physik and Landesforschungszentrum OPTIMAS, Technische Universität Kaiserslautern, 67663 Kaiserslautern, Germany*

(Received 23 December 2022; revised 19 April 2023; accepted 12 May 2023; published 8 June 2023)

We investigate the interaction between surface acoustic waves (SAWs) and spin waves (SWs) in a Pt/Co(2 nm)/Ru(0.85 nm)/Co(2 nm)/Pt compensated synthetic antiferromagnet (SAF) composed of two ferromagnetic layers with equal thicknesses separated by a thin nonmagnetic Ru spacer layer. Because of the combined presence of interlayer dipolar coupling fields and interfacial Dzyaloshinskii–Moriya interaction (iDMI), the optical SW mode shows a large nondegenerate dispersion relation for counter-propagating SWs. Due to resonant SAW-SW interaction, we observe a nonreciprocal SAW transmission in the prepared piezoelectric/SAF hybrid device. We demonstrate that the nonreciprocity of the SAW transmission in symmetric SAFs with equal thicknesses of the magnetic layers can show a substantially different characteristic behavior in comparison to asymmetric SAFs or magnetic single layers with iDMI. For the prepared SAF, the nonreciprocal shift of the magnetoacoustic resonance fields and the magnetoacoustic SW excitation efficiency depend on the external magnetic field sweep direction. For one magnetic field sweep direction and angle of the magnetic field, the resonance fields of the waves propagating in one direction are larger than for the waves propagating in the opposite direction. In addition, the magnitude of the nonreciprocal field shift is at minimum if the external magnetic field is aligned perpendicular to the SW propagation direction. The experimental results are in agreement with a phenomenological SAW-SW interaction model.

DOI: 10.1103/PhysRevB.107.214412

I. INTRODUCTION

Nonreciprocal wave propagation is the key property on which the working principle of rf isolators and circulators is based [1,2]. If wave propagation is nonreciprocal, the properties of the wave in amplitude, phase, or frequency change under an inversion of the wave propagation direction [3]. For spin waves (SWs), amplitude nonreciprocity has been known since the pioneering work of Damon and Eshbach [3,4]. In recent years, the nonreciprocity of the SW dispersion in magnetic layers with Dzyaloshinskii–Moriya interaction and in synthetic antiferromagnets has gained significant interest because it has possible applications in logic and communication devices [3,5–10]. Synthetic antiferromagnets (SAFs) are magnetic bi or multilayers, in which the magnetizations are usually antiferromagnetically coupled by Ruderman–Kittel–Kasuya–Yosida (RKKY)-type indirect interlayer exchange coupling [11,12]. However, nonreciprocal spin-wave devices have not yet found industrial applications owing to the low efficiency of electrical SW excitation/detection and the large SW propagation loss. In contrast to SWs, surface acoustic waves (SAWs) are already widely employed in modern technology, such as in rf bandpass filters in cell phones [13–15]. Efficient excitation and detection of SAWs can be achieved by an rf voltage signal and metallic grating structures—so-called interdigital transducers (IDTs)—on piezoelectric crystals [16]. SAWs do show reciprocal characteristics. This fundamentally limits the possible technological applications of SAWs.

By combining SAWs and SWs in magnetoacoustic devices, such as shown in Fig. 1(a), it is possible to make use of the beneficial properties of both wave types [17]. Due to SAW-SW interaction mechanisms (e.g., magnetostriction) along with the large tunability of the SW dispersion, resonant SAW-SW interaction can be achieved [18–21]. The nonreciprocal properties of the SWs and the nonreciprocity of the magnetoacoustic interaction itself [17] will result in a nonreciprocal wave transmission of the magnetoacoustic device. This yields potential for technological applications, such as magnetoacoustic isolators and circulators. Motivated by these application perspectives, magnetoacoustic samples, loaded with magnetic single layers with interfacial Dzyaloshinskii–Moriya interaction (iDMI) [19,20,22], magnetic bilayers [23,24], and SAFs [25–28] have been in the focus of recent magnetoacoustic studies.

Here, we experimentally characterize the impact of the large nonreciprocity of the SW dispersion of a symmetric Pt/Co(2)/Ru(0.85)/Co(2)/Pt SAF (thicknesses are given in nm) with iDMI and interlayer dipolar coupling (IDC) on the SAW transmission in a piezoelectric/magnetic heterostructure, as depicted in Fig. 1(a). We name antiferromagnetically coupled magnetic bilayers exhibiting a compensated zero net moment at zero field "symmetric bilayer SAFs". For previously studied asymmetric bilayer SAFs [28], magnetic bilayers [23], and magnetic single layers with iDMI [19,20,29], the static magnetization direction and the frequency nonreciprocity switch around zero external magnetic

*matthias.kuess@physik.uni-augsburg.de

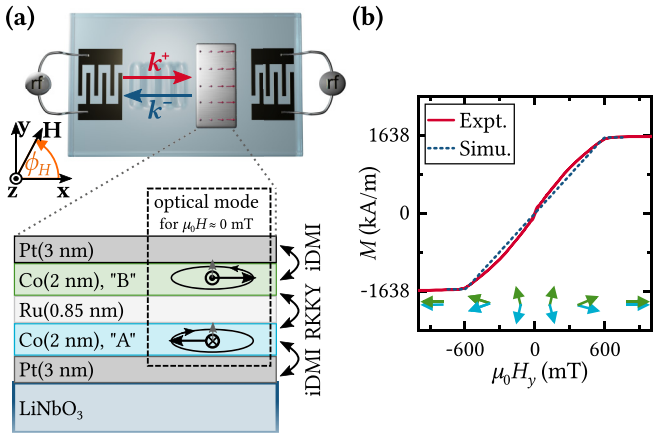

FIG. 1. (a) Illustration of the investigated magnetoacoustic hybrid device and the symmetric layer stack of the Pt/Co(2)/Ru/Co(2)/Pt SAF. The nonreciprocity of the magnetoacoustically excited SWs is characterized by different transmission magnitudes of counter-propagating SAWs with wave vectors k^+ and k^- in dependence of the external magnetic field **H**. For the moderate excitation frequencies of the SAW ($f < 7$ GHz) solely the optical SW mode can be excited. This is schematically shown by the trajectory of the precessing magnetic moments (black arrows) in the Damon-Eshbach geometry at zero field. (b) The *M*-*H* hysteresis loop of the prepared SAF with the magnetic field applied in the *xy* easy magnetization plane along $\phi_H = 90^\circ$. The magnetization hysteresis loops of experiment and simulation agree well. The static configuration of $\mathbf{M}^A$ and $\mathbf{M}^B$ are additionally schematically depicted by the blue and green arrows.

field and are independent of the magnetic field sweep direction. For instance, we recently reported about this behavior for a Pt/Co(2)/Ru(0.85)/Co(4)/Pt asymmetric bilayer SAF with iDMI and IDC [28]. In contrast, we find that the nonreciprocity of symmetric bilayer SAFs can show a substantially different characteristic behavior. First, the magnetization and the frequency nonreciprocity do not switch around zero field. Second, the sign of the frequency nonreciprocity and magnetoacoustic SW excitation efficiency depend on the external magnetic field sweep direction. Third, the magnitude of the nonreciprocally shifted magnetoacoustic resonance fields is at minimum if the external magnetic field is aligned perpendicular to the SW propagation direction. The experimental results are well reproduced by a phenomenological model, which is based on the macrospin approximation and coupled linearized Landau-Lifshitz-Gilbert equations. The symmetric bilayer SAF is a model system for single-phase antiferromagnetic materials.

II. THEORY

Figure 1(a) shows an illustration of the experimental setup and the *xyz* coordinate system used. We will briefly describe the SAW-SW interaction in SAFs consisting of a bottom magnetic layer *A*, a nonmagnetic spacer layer, and a top magnetic layer *B* with a phenomenological model. For details of the theoretical model, we refer to our recent study [28].

The equilibrium in-plane magnetization orientations ϕ_0^l of the magnetizations $\mathbf{M}^l$ are calculated by numeric local energy minimization utilizing a macrospin model [5,30–33]. All polar angles ϕ are defined with respect to the x axis. The wave vectors k of the SAW and SW are given by $\mathbf{k} = k\hat{\mathbf{x}}$. For counter-propagating waves with wave vectors $|k|$, we write k^+ ($k > 0$) and k^- ($k < 0$). If the external magnetic field is aligned in the *xy* plane and the demagnetization fields are larger than the surface anisotropy fields ($M_s^l > H_k$), the equilibrium magnetizations are strictly in-plane and the static energy E_S per surface area can be written as

$$E_S = \sum_{l=A,B} d^l M_s^l \Big[-\mu_0 H \cos\left(\phi_0^l - \phi_H\right) - \frac{1}{2}\mu_0 H_{\text{ani}}^l \cos^2\left(\phi_0^l - \phi_{\text{ani}}^l\right) \Big] - J_{\text{eff}} \cos\left(\phi_0^A - \phi_0^B\right), \tag{1}$$

where we take the Zeeman energy, in-plane uniaxial magnetic anisotropy, and bilinear interlayer exchange coupling into account. For the calculation of the macrospin equilibrium orientations $\mathbf{M}^l$, all the additionally present energy terms have no impact on the in-plane equilibrium orientation, as they vanish for $k = 0$ or are constant. The thicknesses and saturation magnetizations of both magnetic layers are d^l and M_s^l, respectively. Furthermore, H, ϕ_H, H_{ani}^l, and ϕ_{ani}^l are the magnitudes and orientations of the external magnetic field and uniaxial magnetic anisotropies. Antiparallel alignment of $\mathbf{M}^A$ and $\mathbf{M}^B$ is caused by a negative effective interlayer coupling constant $J_{\text{eff}} < 0$. To calculate the equilibrium orientation $\phi_0^l(\mu_0 H)$ for magnetic field up and down sweeps, we use the previous equilibrium directions ϕ_0^l to calculate ϕ_0^l of the successive point of the magnetic field sweep.

The simulated *M*-*H* hysteresis loop of the prepared Pt/Co(2)/Ru(0.85)/Co(2)/Pt SAF with the magnetic field applied in the *xy* easy magnetization plane along $\phi_H = 90^\circ$ is depicted in Fig. 1(b). The static magnetization configuration shows three different magnetic states—namely the ferromagnetic (FM, $\phi_0^A = \phi_0^B$), the canted ($\phi_0^A \neq \{\phi_0^B, \phi_0^B \pm 180^\circ\}$), and the antiferromagnetic ($\phi_0^A = \phi_0^B \pm 180^\circ$) configuration. With decreasing external magnetic field magnitude $|\mu_0 H|$, the magnetic state changes from a ferromagnetic ($|\mu_0 H| \geqslant 600$ mT) to canted (600 mT $> |\mu_0 H| > 0$ mT) to antiferromagnetic ($\mu_0 H = 0$ mT) configuration. Small differences in the parameters of both magnetic layers can determine the rotational sense of $\mathbf{M}^l$ and the equilibrium orientation at $\mu_0 H = 0$ mT. The simulation parameters are summarized in Table I.

For the dynamic magnetoacoustic interaction, we assume that the frequency f and wave vector k of the SAW and excited SWs are identical. The dispersion of the SAW, $f = \frac{1}{2\pi} c_{\text{SAW}}|k|$, is linear and defined by the propagation velocity $c_{\text{SAW}} \approx 3500$ m/s. The SW dispersion of the SAF is calculated from the coupled linearized Landau-Lifshitz-Gilbert (LLG) equations of both magnetic layers. For the effective fields in the LLGs, we consider (i) Zeeman energy, (ii) in-plane uniaxial magnetic anisotropy, (iii) out-of-plane surface anisotropy, (iv) intralayer exchange interaction, (v) intralayer dipolar coupling fields, (vi) iDMI fields, (vii) interlayer bilinear exchange coupling, (viii) interlayer dipolar coupling, and (ix) magnetoacoustic driving fields. The small-amplitude magnetization dynamics of both magnetic layers $l = A, B$ are calculated in individual rotated ($\mathbf{e}_1^l$, $\mathbf{e}_2^l$, $\mathbf{e}_3^l$)

coordinate systems. Hereby, the $\mathbf{e}_3^l$ directions correspond to the equilibrium magnetization orientations, the $\mathbf{e}_2^l$ directions are aligned in the plane of the magnetic film, and the $\mathbf{e}_1^l$ directions are parallel to the film normal. In addition, we assume homogeneous magnetization dynamics along the thickness of both magnetic layers. With the 4×4 magnetic susceptibility tensor, the SW dispersion is obtained by setting $\det(\bar{\chi}^{-1}) = 0$ and taking the real part of the solution [23]. Only the low-frequency SW mode, which we refer to the optical SW mode [5], is relevant for our magnetoacoustic experiments, since the resonance frequency of the high-frequency SW acoustic mode is much higher ($f > 17\,\mathrm{GHz}$) than the SAW excitation frequency (6.82 GHz). This is caused by the antiferromagnetic interlayer exchange coupling. In the limit of identical magnetic layers A and B, antiparallel orientation of $\mathbf{M}^A$ and $\mathbf{M}^B$, zero external magnetic field, and no in-plane uniaxial anisotropy, the SW dispersion yields

$$f(k) = f_0(|k|) + \Delta f_{\mathrm{DMI}}^{\mathrm{IDC}}(k), \tag{2}$$

with

$$\Delta f_{\mathrm{DMI}}^{\mathrm{IDC}}(k) = -\frac{\gamma^A \mu_0}{2\pi}\left(\frac{2D_{\mathrm{eff}}^A}{\mu_0 M_s^A} + \frac{1}{2} d^A M_s^A \zeta^A\right) k \sin\phi_0^A,$$

where γ^l is the gyromagnetic ratio and D_{eff}^l is the thickness-averaged effective DMI constant [34,35]. We define the terms $f_0(|k|)$ and ζ^l in Appendix A. For small $|k|$ ($|k| \ll (d^l)^{-1}, d_s^{-1}$), $\zeta^l \approx 1$. The term $\Delta f_{\mathrm{DMI}}^{\mathrm{IDC}}(k)$, which is proportional to k, lifts the degeneracy of counter-propagating SWs. For $D_{\mathrm{eff}}^A > 0$, the nonreciprocal frequency shift caused by iDMI and IDC adds up. We thus expect a large nonreciprocity $\Delta f_{\pm} = f(k^+) - f(k^-)$ for our sample. With increasing thickness d^l the nonreciprocity caused by iDMI decreases but increases for IDC. In addition, the sign and magnitude of $\Delta f_{\pm}$ depend crucially on the equilibrium orientations ϕ_0^A and $\phi_0^B = \phi_0^A + \pi$ of both magnetic layers. An inversion of the magnetizations $\mathbf{M}^A$ and $\mathbf{M}^B$ will result in a reversed sign of the nonreciprocity. The mode profile of the optical SW mode for the antiparallel alignment of $\mathbf{M}^A$ and $\mathbf{M}^B$ is illustrated in Fig. 1(a).

The propagating SAW modulates the magnetoelastic free energy of the SAF with its frequency and wave vector. This results in an effective magnetoacoustic driving field $\mathbf{h}^l$, which can mediate the SW excitation [36]. The effective magnetoelastic driving field in the $(\mathbf{e}_1^l, \mathbf{e}_2^l)$ plane can be written as a function of SAW power P_{SAW} [20] as

$$\begin{pmatrix} h_1^l \\ h_2^l \end{pmatrix} = \begin{pmatrix} \tilde{h}_1^l \\ \tilde{h}_2^l \end{pmatrix} \sqrt{\frac{k^2}{R\,\omega W}} \sqrt{P_{\mathrm{SAW}}(x)}\, \mathrm{e}^{i(kx-\omega t)}, \tag{3}$$

where W is the width of the aperture of the IDT and R is a constant that depends on the material and crystalline orientation of the substrate. For a Rayleigh SAW on a Y-cut Z-propagation $LiNbO_3$ substrate, we use the numerically calculated constant $R = 1.4 \times 10^{11}\,\mathrm{J/m^3}$ [37]. The x dependence of P_{SAW} takes the attenuation of the SAW due to SAW-SW interaction into account. The normalized effective magnetoelastic driving fields of a Rayleigh wave with strain components $\varepsilon_{ij=xx,xz,zz} \neq 0$ are

$$\begin{pmatrix} \tilde{h}_1^l \\ \tilde{h}_2^l \end{pmatrix} = \frac{2}{\mu_0}\left[b_1^l \tilde{a}_{xx} \begin{pmatrix} 0 \\ \sin\phi_0^l \cos\phi_0^l \end{pmatrix} + b_2^l \tilde{a}_{xz} \begin{pmatrix} \cos\phi_0^l \\ 0 \end{pmatrix}\right]. \tag{4}$$

Here, the magnetoelastic coupling constants for cubic symmetry of the ferromagnetic layers [38,39] are $b_{n=1,2}^l$, $\tilde{a}_{ij} = \varepsilon_{ij,0}/(|k||u_{z,0}|)$ are the normalized amplitudes of the strain, and $\varepsilon_{ij,0}$ are the complex amplitudes of the strain. Moreover, $u_{z,0}$ is the amplitude of the lattice displacement in the z direction. Because the wavelength of the SAW is much larger than the thickness $d^A + d^B$ of both ferromagnetic layers, we assume homogeneous strain along d^l and no change of the waveform of the SAW under SAW-SW interaction. We neglect other nonmagnetoelastic interactions, like spin-rotation coupling [40–42] and gyromagnetic coupling [43]. Magneto-rotation coupling [19,20,44] can phenomenologically be modeled by substituting b_2^l with an effective coupling constant $b_{2,\mathrm{eff}}^l$ [23] and is phenomenologically taken into account by assuming $b_2^l \neq b_1^l$ and $b_2^l \to b_{2,\mathrm{eff}}^l$. The driving field is governed by the equilibrium magnetization orientations ϕ_0^l. Since the longitudinal strain ε_{xx} is the dominating strain component of a Rayleigh SAW, $|\mathbf{h}^l|$ has a four-fold symmetry with maxima at $\phi_0^l = \pm 45^\circ, \pm 135^\circ$ [36]. An approximate estimation of the magnitude of ε_{xx} in our sample gives $\varepsilon_{xx,0} \approx 4 \times 10^{-6}$ [45]. With this value we estimate the maximum driving field magnitude of $h_2^l \approx 20\,\mu\mathrm{T}$ [45] to be small in comparison to the other effective fields present in our SAF, such as the external magnetic field $\mu_0 H \leqslant 1\,\mathrm{T}$.

Besides the SAW-SW resonance condition ($k_{\mathrm{SW}} = k_{\mathrm{SAW}}$, $f_{\mathrm{SW}} = f_{\mathrm{SAW}}$), the driving fields in both magnetic layers determine the total absorbed power P_{abs} of the SAW, caused by SAW-SW interaction. Following Ref. [28], we write

$$P_{\mathrm{abs}} = P_0\left(1 - \exp\left\{-\tilde{C}\,\mathrm{Im}\left[\begin{pmatrix} d^A\tilde{h}_1^A \\ d^A\tilde{h}_2^A \\ d^B\tilde{h}_1^B \\ d^B\tilde{h}_2^B \end{pmatrix}^* \bar{\chi} \begin{pmatrix} \tilde{h}_1^A \\ \tilde{h}_2^A \\ \tilde{h}_1^B \\ \tilde{h}_2^B \end{pmatrix}\right]\right\}\right) \tag{5}$$

with

$$\tilde{C} = \frac{1}{2}\mu_0 l_f \left(\frac{k^2}{R}\right),$$

where l_f is the length of the magnetic thin film along the x axis. With respect to the initial power P_0, the power of the traveling SAW is exponentially decaying while propagating through the magnetic thin film. Finally, to directly simulate the experimentally determined relative change of the SAW transmission ΔS_{ij} on the logarithmic scale, we use

$$\Delta S_{ij} = 10\lg\left(\frac{P_0 - P_{\mathrm{abs}}}{P_0}\right), \quad ij = \begin{cases} 21, & \text{for } k^+ \\ 12, & \text{for } k^- \end{cases} \tag{6}$$

for SAWs propagating parallel (k^+) and antiparallel (k^-) to the x axis.

III. EXPERIMENTAL SETUP

We used magnetron sputter deposition for the preparation of the Pt(3)/Co(2)/Ru(0.85)/Co(2)/Pt(3)/Si_3N_4(3) SAF on a piezoelectric Y-cut Z-propagation $LiNbO_3$ substrate. Especially strong antiferromagnetic interlayer exchange coupling has been observed in such multilayers made out of Co/Ru(d_s)/Co for $0.5\,\mathrm{nm} \lesssim d_s \lesssim 1\,\mathrm{nm}$ [30,46,47]. Moreover, the Pt layers cause iDMI in Co [48–50]. For SAW

excitation and detection, we use a pair of interdigital transducers, which have three finger pairs with a periodicity of 3.4 μm and can be operated up to ∼7 GHz. The Y-cut Z-propagation $LiNbO_3$ substrate gives rise to Rayleigh-type SAW excitation [14]. More details about the IDT geometry and preparation of the SAF are presented in Refs. [20,28].

We measured the *M*-*H* hysteresis loop of the prepared SAF by superconducting quantum interference device-vibrating sample magnetometry (SQUID-VSM) with the external magnetic field aligned in the plane of the thin film along the *y* axis and for the magnetic field up and down sweep. The results are presented in Fig. 1(b) and show the expected linear behavior $M(H)$ of the canted magnetization state.

An additional Pt(3)/Co(2)/Ru(0.85)/Si_3N_4(3) reference sample consisting of a single magnetic Co layer was prepared. On this sample SQUID-VSM magnetometry and broadband ferromagnetic-resonance (bbFMR) measurements were performed to further study the magnetic properties.

We use a vector network analyzer to characterize the SAW transmission at 6.82 GHz, corresponding to the seventh harmonic operation of our delay line device. A time-domain gating technique was employed to exclude spurious signals [51], in particular, electromagnetic crosstalk. We use the relative change of the background-corrected SAW transmission signal

$$\Delta S_{ij}(\mu_0 H) = S_{ij}(\mu_0 H) - S_{ij}(800\,\mathrm{mT}) \tag{7}$$

to characterize SAW-SW coupling. Here, ΔS_{ij} is the magnitude of the complex transmission signal with $ij = 21, 12$. In all measurements, we perform either magnetic field up sweeps (−800 mT to +800 mT) or down sweeps (+800 mT to −800 mT) with maximum field magnitudes high enough to ensure full magnetic saturation.

IV. EXPERIMENTAL RESULTS

In Fig. 2(a), we show the magnetoacoustic transmission $\Delta S_{ij}(\mu_0 H)$ of the prepared Pt/Co/Ru/Co/Pt SAF for the magnetic field up sweep and fixed field orientation of $\phi_H = 32.4^\circ$. The SAW-SW resonance fields are clearly shifted by $\Delta|\mu_0 H_{\mathrm{res}}|_\pm = |\mu_0 H_{\mathrm{res}}^{S21}| - |\mu_0 H_{\mathrm{res}}^{S12}|$ for counter-propagating magnetoacoustic waves with wave vectors k^+ and k^-. In contrast to previous reports about magnetic films with iDMI and IDC [20,23,28,29,52], the sign of this nonreciprocal splitting $\Delta|\mu_0 H_{\mathrm{res}}|_\pm$ is identical for $\mu_0 H < 0$ and $\mu_0 H > 0$. If the magnetic field sweep direction is inverted, the sign of $\Delta|\mu_0 H_{\mathrm{res}}|_\pm$ changes, as shown in Fig. 2(b). For the so far studied magnetic single layers with iDMI or magnetic bilayers the magnetic field sweep direction did not have an impact on the nonreciprocity $\Delta|\mu_0 H_{\mathrm{res}}|_\pm$ [20,23,28,29].

Additionally, we present in Figs. 3(a)–3(d) for inverted wave vectors $k^\pm$ and inverted magnetic field sweep directions the magnetoacoustic transmission $\Delta S_{ij}(\mu_0 H, \phi_H)$ as a function of the external magnetic field magnitude and orientation. The dashed lines at $\phi_H = 32.4^\circ$ show the scans along the linecuts displayed in Fig. 2. The nonreciprocal splitting of the resonance fields $|\Delta|\mu_0 H_{\mathrm{res}}|_\pm|$ decreases with increasing $|\phi_H|$. For magnetic single layers with iDMI or asymmetric magnetic bilayers, increasing $|\Delta|\mu_0 H_{\mathrm{res}}|_\pm|$ is usually observed if $|\phi_H|$ is increased with $|\phi_H| \leqslant 90^\circ$ [3,20,23,28,29,49]. Moreover,

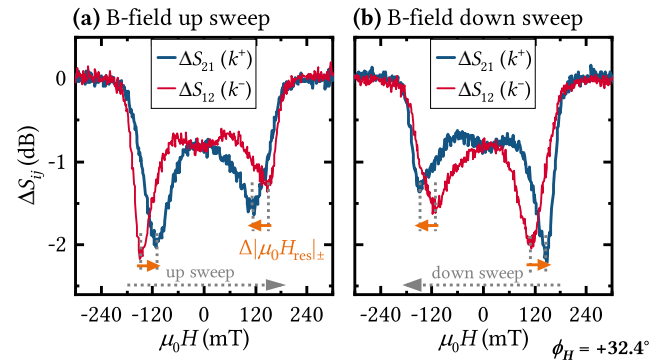

FIG. 2. (a) Transmission magnitude ΔS_{21} and ΔS_{12} of counter-propagating SAWs with wave vectors k^+ and k^- at 6.82 GHz. The external magnetic field is aligned at $\phi_H = 32.4^\circ$ and increased from −800 mT to +800 mT, which is indicated by the gray dashed arrow. The resonance fields of ΔS_{21} and ΔS_{12} are nonreciprocally shifted by $\Delta|\mu_0 H_{\mathrm{res}}|_\pm$. In contrast to previous studies [20,23,28,29,52], the resonance fields $|\mu_0 H_{\mathrm{res}}|$ of ΔS_{21} are for positive *and* negative magnetic fields, lower than for ΔS_{12}. (b) The nonreciprocal field shift $\Delta|\mu_0 H_{\mathrm{res}}|_\pm$ gets inverted under an inversion of the magnetic field sweep direction (+800 mT to −800 mT).

for positive fields $\mu_0 H > 0$ and the magnetic field up sweep, the SAW-SW resonances in Figs. 3(a) and 3(b) are shifted to larger $|\phi_H|$ than for $\mu_0 H > 0$ and the magnetic field down sweep in Figs. 3(c) and 3(d).

In addition to the resonance at $\mu_0 H \approx \pm 120$ mT, we observe a high-field resonance with lower intensity at $\mu_0 H \approx \pm 560$ mT. The nonreciprocal field shift of this resonance is low ($|\Delta|\mu_0 H_{\mathrm{res}}|_\pm| \lesssim 7$ mT, see Appendix C) in comparison to the resonances at $\mu_0 H \approx \pm 120$ mT ($|\Delta|\mu_0 H_{\mathrm{res}}|_\pm| \lesssim 43$ mT).

V. DISCUSSION

The simulations in Figs. 3(e)–3(h) were carried out using Eq. (6) of the theory section. The simulation and experiment displayed in Fig. 3 show a rather good quantitative agreement with respect to all salient features such as resonance fields, linewidth, nonreciprocity, and transmission magnitude. The parameters used for all simulations in this study are summarized in Table I. More information about the parameters is given in Appendix B.

Similar to our results, Matsumoto *et al.* observed recently [27] that the amplitude of the SAW transmission magnitude of a symmetric CoFeB(20)/Ru(0.46)/CoFeB(20) SAF at 1.4 GHz is for positive and negative fields $\mu_0 H$ generally larger for magnetoacoustic waves with positive wave vectors k^+ than for negative wave vectors k^-. Because the authors did not observe shifted SAW-SW resonances for counter-propagating waves, which would clearly indicate a nonreciprocal SW dispersion, they conclude that a nonuniform magnetic structure along the film normal of the relatively thick layer stack might explain their results. The physics observed here using a Pt/Co(2)/Ru(0.85)/Co(2)/Pt SAF with relatively low thickness and nonreciprocally shifted resonance fields are qualitatively different and can be accounted for by a homogeneous magnetic structure.

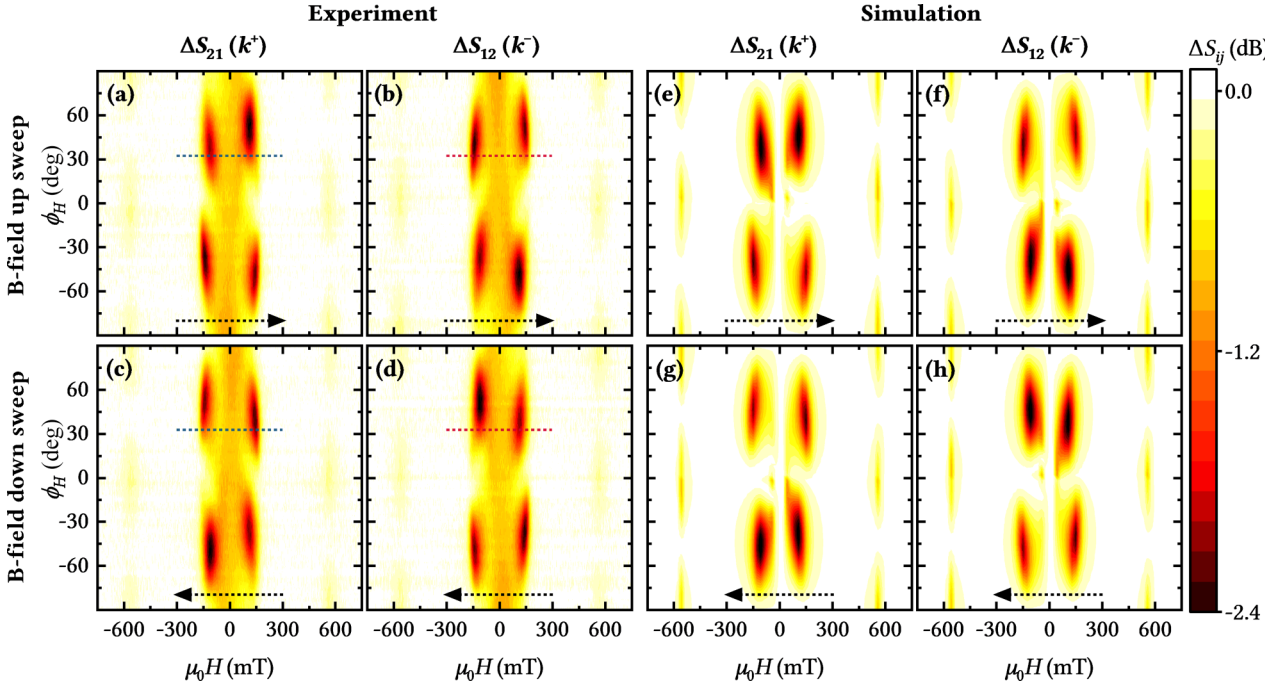

FIG. 3. Change of the SAW transmission $\Delta S_{ij}(\mu_0 H, \phi_H)$ as a function of the external magnetic field magnitude and orientation at 6.82 GHz for (a), (b) magnetic field up sweeps and (c), (d) magnetic field down sweeps. The dashed blue and red lines indicate the position of the linecuts displayed in Fig. 2. In comparison to the low-field resonances at $\mu_0 H \approx \pm 120$ mT, the nonreciprocal field shift of the high-field resonances at $\mu_0 H \approx \pm 560$ mT is low ($|\Delta|\mu_0 H_{\mathrm{res}}|_{\pm}| \lesssim 7$ mT). Experiments (a)–(d) and simulations (e)–(h) show good overall agreement.

In the next section, we will discuss the unusual nonreciprocal behavior and the symmetry of the magnetoacoustic driving fields of the symmetric Pt/Co/Ru/Co/Pt SAF.

A. Nonreciprocity of the SW dispersion

Resonant magnetoacoustic interaction is, in principle, possible where the frequency and wave vector of the SAW and SW match. Therefore, we first calculated the SW resonance frequencies $f(\mu_0 H, \phi_H)$ for the wave vector $k = 13.2\,\mu\mathrm{m}^{-1}$ of the SAW as a function of the external field magnitude and direction. The frequency of the SAW is constant with $f = 6.82$ GHz. The results are presented in Fig. 4 for inverted wave vectors $k^{\pm}$ and inverted magnetic field sweep directions. The resonance positions of the experimental results in Fig. 3 agree well with the SAW-SW resonance condition, which is indicated by the yellow color in Fig. 4. Therefore, the unusual nonreciprocal behavior of the magnetoacoustic transmission ΔS_{ij} can be traced back to the unusual nonreciprocal behavior of the SW dispersion and is not caused by the SAW-SW helicity mismatch effect [19,20,38,55]. The field sweep direction affects the equilibrium magnetization directions ϕ_0^l and the SW resonance frequency. We will now discuss the nonreciprocity of the SW resonance frequencies $f(\mu_0 H, \phi_H)$ and the impact of the magnetic field sweep direction on the nonreciprocity of $f(\mu_0 H, \phi_H)$ in more detail.

1. Impact of iDMI and IDC on the nonreciprocity of the optical SW mode

We calculated in Fig. 5(a) the SW resonance frequency $f(\mu_0 H)$ for the magnetic field up sweep and fixed magnetic field direction of $\phi_H = 18^\circ$. These curves are scans along the linecuts of Fig. 4, where the positions of the linecuts are indicated by the dashed gray lines. Additionally, we show in Figs. 5(b) and 5(c) the corresponding nonreciprocity $\Delta f_{\pm}(k) = f(k^+) - f(k^-)$ of the SW resonance frequency and the magnetization equilibrium orientations ϕ_0^l of both magnetic layers A and B. The orientations ϕ_0^l are uniquely identifiable because of small differences in the properties of

TABLE I. Summary of the parameters used for all simulations of ΔS_{21} (k^+). For the simulation of ΔS_{12} (k^-), the sign of the normalized strain $\tilde{a}_{xz}$ is inverted [20]. Furthermore, the bilinear interlayer exchange coupling constant $J_{\mathrm{eff}} = -0.95\,\mathrm{mJ/m^2}$ is extracted from the M-H magnetization hysteresis and we assume $c_{\mathrm{SAW}} = 3240$ m/s [53] for the SAW propagation velocity in the SAF. The length of the SAF along the SAW propagation direction is $l_f = 750\,\mu$m.

	Layer l	d^l (nm)	g^l	M_s^l (kA/m)	H_k^l (kA/m)	A_{ex}^l (pJ/m)	D_{eff}^l (mJ/m^2)	$\mu_0 H_{\mathrm{ani}}^l$ (mT)	ϕ_{ani}^l (°)	α^l	$b_1^l \tilde{a}_{xx}$ (T)	$b_2^l \tilde{a}_{xz}$ (T)
Co(2)	B	2	2.317	1620	1085	31 [5,54]	−0.70	4	0	0.071	1.9	0.42i
Co(2)	A	2	2.317	1580	1085	31 [5,54]	+0.70	0	0	0.071	1.9	0.42i

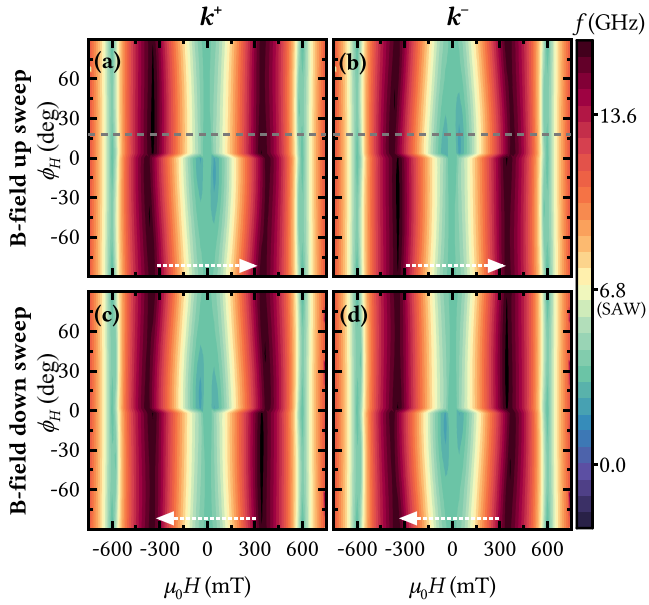

FIG. 4. Spin wave resonance frequencies $f(\mu_0 H, \phi_H)$ for SWs with inverted propagation directions $k^{\pm}$ and magnetic field up and down sweeps. Resonant SAW-SW interaction is potentially possible at 6.82 GHz (yellow color). The SW dispersion was calculated for the wave vector $|k| = 13.2\,\mu\text{m}^{-1}$ of a 6.82 GHz SAW. The gray dashed lines indicate the position of the line-cuts which are shown in Fig. 5(a).

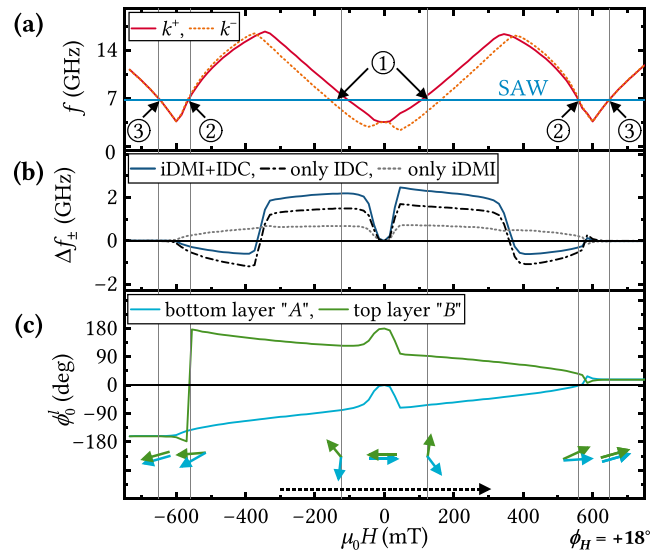

FIG. 5. (a) The calculated resonance frequency of the optical SW mode for the magnetic field up sweep shows nondegenerated frequencies for counter-propagating SWs with wave vectors k^+ and k^-. Resonant SAW-SW interaction is potentially possible at $|\mu_0 H_{\text{res}}| \approx$ 120, 560, and 650 mT. These resonances are labeled as ①, ②, and ③. (b) The large frequency nonreciprocity $\Delta f_{\pm} = f(k^+) - f(k^-)$ of the SAF is caused by iDMI and IDC (iDMI+IDC). This can be understood as an additive interplay of both individual contributions of iDMI and IDC [5]. (c) The equilibrium orientations ϕ_0^l of the magnetizations $\mathbf{M}^l$, which are schematically depicted by arrows for the magnetoacoustic resonance fields and zero field govern $f(\mu_0 H)$. While $\Delta f_{\pm}$ is large in the canted configuration, $\Delta f_{\pm}$ is zero in the ferromagnetic configuration ($\phi_0^A = \phi_0^B$). All calculations were carried out for $\phi_H = 18^\circ$.

both magnetic layers of the SAF (see Table I for details), which in turn determine the sign of $\Delta f_{\pm}(k)$. The SW resonance frequency $f(\mu_0 H)$ shows minima, where the static magnetization configuration changes from a ferromagnetic to a canted configuration at $\mu_0 H \approx \pm 600$ mT and around zero field.

The SAW-SW resonance fields in Fig. 5(a) at $|\mu_0 H_{\text{res}}| \approx$ 120, 560, and 650 mT are labeled as ①, ②, and ③, respectively. In agreement with the experimental results in Fig. 3 we observe resonances at positions ① and ②. But the experiment does not show a resonance in the ferromagnetic configuration of the SAF at position ③. This can be attributed to a vanishing magnetoacoustic SW excitation efficiency, as detailed later.

The SW resonance $f(\mu_0 H)$ in Fig. 5(a) shows a large frequency nonreciprocity $\Delta f_{\pm}$ in the canted configuration at $|\mu_0 H| \lesssim 370$ mT. For larger fields $|\mu_0 H|$, the nonreciprocity $\Delta f_{\pm}$ decreases. This is in agreement with the nonreciprocal field shift $\Delta|\mu_0 H_{\text{res}}|_{\pm}$ in the experiment. Only for the low-field magnetoacoustic resonance ①, we observe in Fig. 3 a large $\Delta|\mu_0 H_{\text{res}}|_{\pm}$.

The reason for the large frequency nonreciprocity $\Delta f_{\pm}$ in the canted configuration is characterized in Fig. 5(b). Since iDMI and IDC are wellknown to cause frequency nonreciprocity, the impact of both individual contributions on $\Delta f_{\pm}$ is calculated by setting the corresponding other effective field to zero [28]. A constructive superposition of $\Delta f_{\pm}$ caused by iDMI and IDC results in a very large frequency nonreciprocity of more than 2 GHz at resonance ①. Furthermore, the impact of iDMI of the top and bottom ferromagnetic layer on $\Delta f_{\pm}$ is expected to have additive contributions [5] in the almost antiferromagnetic configuration of the SAF at resonance ①.

The nonreciprocity $\Delta f_{\pm}$ is significantly lowered at $|\mu_0 H| \gtrsim$ 370 mT due to destructive superposition of $\Delta f_{\pm}$ caused by iDMI and IDC. Finally, $\Delta f_{\pm}$ is zero in the FM configuration of the symmetric bilayer SAF. For asymmetric bilayer SAFs in the FM configuration, the nonreciprocity $\Delta f_{\pm}$ does not usually vanish [3,5,23,28]. A detailed theoretical discussion about the enhancement of $\Delta f_{\pm}$ in different antiferromagnetically coupled magnetic bilayers with iDMI and IDC was recently presented by A. Franco and P. Landeros [5].

2. *Impact of the coherent magnetization reversal on the SAW transmission*

The coherent magnetization reversal of a symmetric bilayer SAF has a crucial impact on the nonreciprocity of resonance ①. As shown in Fig. 5(c), the main magnetization rotation of $\mathbf{M}^B$ ($\mathbf{M}^A$) is clockwise (counterclockwise) and coherent without an inversion of the antiparallel alignment of both magnetizations around zero field. In Fig. 6, we additionally illustrated the coherent reversal and the resonance positions ① of $\mathbf{M}^A$ and $\mathbf{M}^B$ for different magnetic field sweep geometries. For the sake of simplicity, we do not show the alignment of $\mathbf{M}^l$ around zero field. At resonance ①, the magnetizations $\mathbf{M}^A$ and $\mathbf{M}^B$ are almost antiferromagnetically aligned ($|\phi_0^A - \phi_0^B| \approx 160^\circ$) perpendicular to the external magnetic field direction. The magnetic field orientation ϕ_H, field sweep direction, and the assumed dominating small in-plane uniaxial

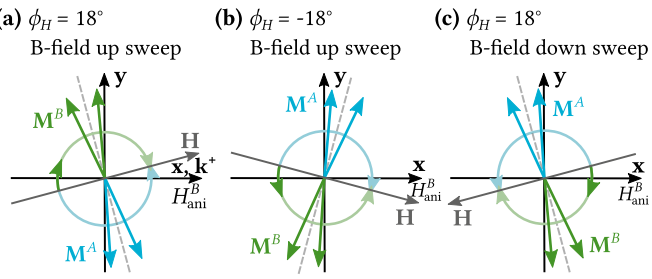

FIG. 6. Illustration of the coherent macrospin magnetization reversal $\mathbf{M}^{A,B}(\mu_0 H)$ for different directions of the external magnetic field $\phi_H = \pm 18^\circ$ and magnetic field up and down sweeps. The orientation of $\mathbf{H}$ for positive fields $\mu_0 H > 0$ is indicated by the tip of the gray arrow. At the beginning of the magnetization reversal, $\mathbf{M}^A$ and $\mathbf{M}^B$ are both aligned antiparallel to the gray arrow (saturation for $\mu_0 H < 0$). With increasing $\mu_0 H$ both magnetizations align canted to each other. The rotation direction is determined by the dominating assumed in-plane uniaxial easy axis direction H^B_{ani} of layer B along the x axis. For the sake of simplicity we do not show the alignment of $\mathbf{M}^l$ around zero field [see, e.g., Fig. 5(c)]. The reversal of $\mathbf{M}^{A,B}(\mu_0 H)$ is indicated by the circular arrows. For the resonances ① at $\mu_0 H \approx \pm 120$ mT, the orientation of both macrospins $\mathbf{M}^A$ (blue arrow) and $\mathbf{M}^B$ (green arrow) are illustrated. Here, $\mathbf{M}^{A,B}$ are almost antiparallel to each other and perpendicular to the magnetic field (gray dashed line).

easy-axis field H^B_{ani} of layer B along the x axis determine the rotational sense of $\mathbf{M}^l$. The assumed difference between M^A_s and M^B_s (see Table I) is too small to have a significant impact on the rotational sense of $\mathbf{M}^l$. The nonreciprocity of a symmetric bilayer SAF in the antiferromagnetic configuration can be described by Eq. (2) with $\Delta f_\pm \propto k \sin \phi^B_0$.

In Fig. 6(a), we discuss the results for the magnetic field up sweep at $\phi_H = 18^\circ$. For negative and positive SAW-SW resonance fields at resonance ①, the macrospin $\mathbf{M}^B$ stays in the same quadrant ($\sin \phi^B_0 > 0$); therefore, the resonance frequencies of SWs with k^+ are larger than that of SWs with k^-, and the SAW-SW resonance fields are lower for magnetoacoustic waves with k^+ than for that with k^-, as observed in Fig. 2(a). Thus, the magnitude and sign of the nonreciprocal field shift $\Delta|\mu_0 H_{\text{res}}|_\pm$ from the experiment is related to the orientation of the macrospins $\mathbf{M}^l$ including the coherent magnetization reversal without an inversion of the antiparallel alignment of both magnetizations around zero field. In contrast, for asymmetric bilayer SAFs (magnetic thin films) made from a soft magnetic material, the equilibrium magnetization orientation usually gets inverted around zero field because the magnetization of the thicker magnetic layer (magnetic single layer) aligns along the external magnetic field direction. Thus, for these magnetic systems, the sign of the nonreciprocity $\Delta f_\pm$ and the nonreciprocal field shift $\Delta|\mu_0 H_{\text{res}}|_\pm$ are inverted for $\mu_0 H > 0$ and $\mu_0 H < 0$ [19,20,28,29].

In the experimental results in Fig. 3 the nonreciprocity $|\Delta|\mu_0 H_{\text{res}}|_\pm|$ of resonance ① at $\mu_0 H \approx \pm 120$ mT decreases with increasing $|\phi_H|$. Because of iDMI and IDC, the nonreciprocity $|\Delta f_\pm|$ of the optical SW mode in the antiferromagnetic configuration of the SAF is large for the configuration $\mathbf{M}^l \perp \mathbf{k}$ and small for $\mathbf{M}^l \parallel \mathbf{k}$. Here, since both $\mathbf{M}^l$ are essentially orthogonal to $\mathbf{H}$ (see Fig. 6), we have to apply $\mathbf{H}$ along $\mathbf{k}$ to get the large nonreciprocity.

While the reversal of $\mathbf{M}^B$ is clockwise in Fig. 6(a) at $\phi_H = 18^\circ$, it is because of of the small in-plane anisotropy of layer B, and according to Eq. (1) counterclockwise in Fig. 6(b) at $\phi_H = -18^\circ$. As a consequence, at the resonance ①, the sign of ϕ^B_0 in Figs. 6(a) and 6(b) differs ($-180^\circ \leqslant \phi^l_0 < 180^\circ$). Thus, the signs of the frequency nonreciprocity $\Delta f_\pm$ and the nonreciprocal field shift $\Delta|\mu_0 H_{\text{res}}|_\pm$ are inverted for magnetic field sweeps with $\phi_H > 0$ and $\phi_H < 0$. We observe this behavior in experiment and theory shown in Figs. 3 and 4.

3. Impact of the magnetic field sweep direction on the nonreciprocity

The experimental transmission measurements in Figs. 2 and 3 demonstrate that an inversion of the field sweep direction results in an inversion of the nonreciprocal field shift $\Delta|\mu_0 H_{\text{res}}|_\pm$. While $\mathbf{M}^B$ rotates clockwise in the upper xy half-plane ($\sin \phi^B_0 \gtrsim 0$) for the magnetic field up sweep in Fig. 6(a), it rotates clockwise in the lower xy half-plane ($\sin \phi^B_0 \lesssim 0$) for the field down sweep in Fig. 6(c). This hysteretic magnetization rotation is caused by the dominating in-plane uniaxial easy axis direction H^B_{ani} of layer B along the x axis. Therefore, the frequency nonreciprocity $\Delta f_\pm \propto k \sin \phi_B$ and the nonreciprocal field shift $\Delta|\mu_0 H_{\text{res}}|_\pm$ get inverted under an inversion of the field sweep direction. For the sake of simplicity, we assume $H^A_{\text{ani}} = 0$. We obtain similar good agreement between experiment and simulation for $H^A_{\text{ani}} \neq 0$ if H^B_{ani} is about 4 mT larger than H^A_{ani}.

B. Symmetry of the magnetoacoustic driving fields

Besides the nonreciprocal splitting of the resonance fields $\Delta|\mu_0 H_{\text{res}}|_\pm$, the magnetic field sweep direction has also an impact on the intensity of the SAW-SW resonances. For positive fields ($\mu_0 H > 0$), the SAW-SW resonances in Figs. 3(a)–3(d) are shifted to larger $|\phi_H|$ for the magnetic field up sweep in comparison to the magnetic field down sweep. We attribute this hysteretic behavior to the symmetry of the effective magnetoacoustic driving fields in both magnetic layers of the SAF. In Figs. 7(a)–7(d) we show the dominating magnetoelastic driving field h^l_2, which is caused by the longitudinal strain ε_{xx} of the Rayleigh type SAW for both magnetic layers of the SAF. Because the coherent magnetization reversal $\phi^l_0(\mu_0 H)$ is hysteretic, as discussed in the previous section, the symmetry of the driving fields differ for the magnetic field up and down sweep. The coherent magnetization reversal of $\mathbf{M}^A$ and $\mathbf{M}^B$ results in an almost mirror symmetry behavior of h^A_2 and h^B_2. This symmetry gets broken if the strain ε_{ij} or the magnetic properties (d^l, M^l_s, H^l_{ani}, ϕ^l_{ani}, b^l_1) of both magnetic layers differ. Here, we assume that the in-plane uniaxial magnetic anisotropies and the saturation magnetizations of both magnetic layers are slightly different (details in Table I) [56]. Thus, the sum of the driving fields $|h^A_2 + h^B_2|$ which was calculated in Figs. 7(e) and 7(f) shows an asymmetric behavior with respect to $\mu_0 H = 0$. For the SAW-SW resonance ①, $\mathbf{M}^A$ and $\mathbf{M}^B$ are almost antiferromagnetically aligned. Since the total magnetoacoustic driving efficiency of the optical SW mode in the antiferromagnetic configuration of the symmetric bilayer SAF is approximately given by $|h^A_2 + h^B_2|$ [28], the intensity of

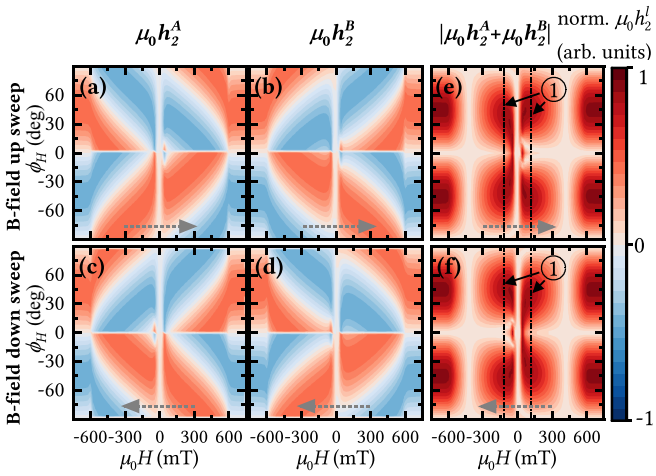

FIG. 7. (a)–(d) The calculated in-plane magnetoacoustic driving field magnitude $\mu_0 h_2^l(\mu_0 H, \phi_H)$ in the bottom (A) and top magnetic layer (B) of the SAF is shown for the magnetic field up and down sweep. For the SAW-SW resonance fields at $\mu_0 H \approx \pm 120$ mT (①), the magnetizations $\mathbf{M}^A$ and $\mathbf{M}^B$ are almost antiparallel aligned to each other. In this configuration, efficient magnetoacoustic excitation of the optical SW mode is possible if $|\mu_0 h_2^A + \mu_0 h_2^B|$ is large. (e) and (f) The sum of the driving fields $|\mu_0 h_2^A + \mu_0 h_2^B|$ shows an asymmetric behavior with respect to $\mu_0 H = 0$ and differs for the magnetic field up and down sweeps. Thus, the SAW transmission magnitude of resonance ① depends on the field sweep direction, as observed in Fig. 3. The magnitude of the driving fields was normalized to $\max(\mu_0 h_2^A + \mu_0 h_2^B)$.

the resonances in Fig. 3 follows the asymmetry of $|h_2^A + h_2^B|$. This asymmetry only depends on the magnetic field sweep direction, as observed in Fig. 3. Note that for macrospins $\mathbf{M}^A$ and $\mathbf{M}^B$ with a large canting angle or ferromagnetic alignment, the sum $|h_2^A + h_2^B|$ does not describe the magnetoacoustic driving efficiency.

In Fig. 5(a), there are three SW-SAW dispersion crossings ①, ②, and ③ for any k direction. In the experiment in Fig. 3, we obtain SAW absorption for only the two crossings ① and ②. The coupling efficiency between the SAW and optical SW mode of the crossing ③ is zero, because the symmetric bilayer SAF with identical magnetoelastic coupling constants $b_n^A = b_n^B$ and SAW strain $\tilde{a}_{ij}^A = \tilde{a}_{ij}^B$ is in pure FM configuration. The coupling efficiency is already very weak for the crossing ② because the $\mathbf{M}^A$ and $\mathbf{M}^B$ are almost ferromagnetically aligned there. The model describes the SAW-SW coupling efficiency by taking in Eq. (5) the phases of the magnetoacoustic driving fields $\mathbf{h}^l$ and magnetizations precession $\bar{\chi}\mathbf{h}^l$ in both magnetic layers into account. Note that for magnetic bilayers made from different magnetic materials the sign and magnitude of b_n^A and b_n^B determine the coupling efficiency between the SAW and optical/acoustic SW mode. For instance, the coupling between the SAW and optical SW mode in the FM configuration of a magnetic bilayer is expected to be very large for $\mathrm{sgn}\,(b_n^A) \neq \mathrm{sgn}\,(b_n^B)$ and has been demonstrated to be large for $b_n^A \approx 0$, $b_n^B \neq 0$ in a NiFe/Au/CoFeB magnetic bilayer [23].

Besides the nonreciprocity of the SW dispersion, another mechanism, which is based on a helicity mismatch between the driving fields and magnetizations precession [19,20,38,55] can cause a nonreciprocal amplitude of the SAW transmission. For the symmetric bilayer SAF with identical magnetoelastic coupling constants $b_2^A = b_2^B$, we do not observe the SAW-SW helicity mismatch effect, since the total impact of the out-of-plane driving fields $\tilde{h}_1^l$ on the magnetizations precession cancels for the optical SW mode excitation.

VI. CONCLUSIONS

In summary, we have studied the SAW-SW interaction in a symmetric Pt/Co(2)/Ru/Co(2)/Pt SAF. Our experiments are in good agreement with analytical model calculations. The nonreciprocity caused by IDC and iDMI at the top and bottom ferromagnetic Co layer adds up for the optical SW mode in the canted configuration of the SAF around zero field. The resulting large nonreciprocity of the SW dispersion of more than 2 GHz causes nonreciprocally shifted resonance fields for magnetoacoustic transmission measurements, which were carried out at a constant SAW excitation frequency of 6.82 GHz. While the nonreciprocal shift of the resonance fields is large, the maximum nonreciprocity of the SAW transmission magnitude $\Delta S_\pm = |\Delta S_{21} - \Delta S_{12}| \approx 1.5$ dB is moderate in comparison to magnetic bilayers and SAFs with low-damping and thicker ferromagnetic layers ($\Delta S_\pm \approx 30$ dB) [23,24,27].

In addition, the nonreciprocity of the SW resonance fields shows a significantly different behavior in comparison to asymmetric bilayer SAFs or magnetic single layers with iDMI, because of coherent magnetization reversal and different in-plane uniaxial magnetic anisotropies of both ferromagnetic layers of the SAF. For the prepared SAF, we find that the sign of the frequency nonreciprocity depends on the external magnetic field sweep direction and is identical for positive and negative magnetic fields. Furthermore, for the symmetric bilayer SAF, the external magnetic field sweep direction has an impact on the magnitude of the magnetoacoustic SW excitation efficiency. We find that the excitation efficiency of SWs in the canted configuration around zero field is large and at maximum for $\phi_H \approx \pm 45^\circ$. Finally, our experimental observations of magnetoacoustic coupling in symmetric bilayer SAF structures constitute a step toward exploring magnetoacoustic interactions in single-phase antiferromagnets.

ACKNOWLEDGMENTS

This work is funded by the Deutsche Forschungsgemeinschaft (DFG, German Research Foundation) Project No. 492421737.

APPENDIX A: SPIN WAVE DISPERSION OF A SYMMETRIC BILAYER SAF IN THE ANTIFERROMAGNETIC CONFIGURATION

In Eq. (2) we have calculated the SW dispersion of a magnetic bilayer SAF in the limit of identical magnetic layers, antiparallel orientation of $\mathbf{M}^A$ and $\mathbf{M}^B$, zero external magnetic field, and zero in-plane uniaxial anisotropy.

Furthermore, we assume $D^B_{\text{eff}} = -D^A_{\text{eff}}$ because of the symmetry of the SAF [57]. The term f_0 is given by

$$f_0(|k|) = \frac{\gamma\mu_0}{2\pi}\Bigg[\left(-H_k + Dk^2 + M_s G_0 - \frac{1}{2}dM_s\zeta|k| - \frac{2J_{\text{bl}}}{\mu_0 M_s d}\right)\left(Dk^2 + M_s(1-G_0)\sin^2\phi_0 - \frac{1}{2}dM_s\zeta|k|\sin^2\phi_0\right)\Bigg]^{\frac{1}{2}} \tag{A1}$$

with $D = \frac{2A_{\text{ex}}}{\mu_0 M_s}$, $G_0 = \frac{1-e^{-|k|d}}{|k|d}$, and $\zeta = (G_0)^2 e^{-|k|d_s}$. Here, all variables refer to the parameters of layer A. Note, that a small external magnetic field or in-plane uniaxial anisotropies, which are of similar magnitude as the terms under the square-root, will have a large impact on the SW dispersion.

APPENDIX B: SIMULATION PARAMETERS

The parameters used for all simulations in this study are summarized in Table I. Hereby, the saturation magnetization $M^A_s = 1580\,\text{kA/m}$ was taken from the SQUID-VSM measurement of the Pt(3)/Co(2)/Ru(0.85)/Si_3N_4(3) reference sample. M^B_s of the top layer is assumed to be slightly larger (2.5%) than M^A_s. The g-factors, surface anisotropy fields H^l_k, and effective SW damping constants α^l, which considers Gilbert damping and inhomogeneous line broadening [20], were determined by bbFMR measurements, performed on the reference sample. Moreover, the magnetic exchange constants A^l_{ex} and effective DMI-constants D^l_{eff} are taken from the literature [5,28,54]. The parameters of the in-plane uniaxial easy axis and the driving fields $b^l_1\tilde{a}_{xx}$ and $b^l_2\tilde{a}_{xz}$ are identical to our previously studied Pt/Co(2)/Ru/Co(4)/Pt asymmetric SAF [28].

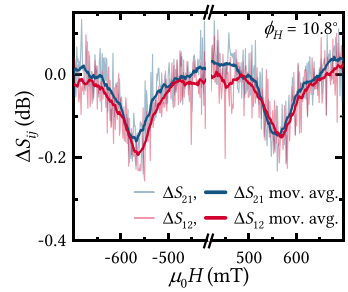

FIG. 8. Transmission magnitude ΔS_{21} and ΔS_{12} at 6.82 GHz. The external magnetic field is aligned at $\phi_H = 10.8^\circ$ and increased from −800 mT to +800 mT.

APPENDIX C: SUPPLEMENTAL FIGURE

In Fig. 8 we show scans along the linecuts of Figs. 3(a) and 3(b) at $\phi_H = 10.8^\circ$. The nonreciprocal field shift of the high-field resonance at $\mu_0 H \approx \pm 560\,\text{mT}$ is low ($|\Delta|\mu_0 H_{\text{res}}|_\pm| \lesssim 7\,\text{mT}$) in comparison to the resonances at $\mu_0 H \approx \pm 120\,\text{mT}$ ($|\Delta|\mu_0 H_{\text{res}}|_\pm| \lesssim 43\,\text{mT}$).

[1] C. E. Fay and R. L. Comstock, Operation of the ferrite junction circulator, IEEE Trans. Microwave Theory Techn. **13**, 15 (1965).

[2] J. D. Adam, L. E. Davis, G. F. Dionne, E. F. Schloemann, and S. N. Stitzer, Ferrite devices and materials, IEEE Trans. Microwave Theory Tech. **50**, 721 (2002).

[3] R.A. Gallardo, T. Schneider, A.K. Chaurasiya, A. Oelschlägel, S.S.P.K. Arekapudi, A. Roldán-Molina, R. Hübner, K. Lenz, A. Barman, J. Fassbender, J. Lindner, O. Hellwig, and P. Landeros, Reconfigurable Spin-Wave Nonreciprocity Induced by Dipolar Interaction in a Coupled Ferromagnetic Bilayer, Phys. Rev. Appl. **12**, 034012 (2019).

[4] R. W. Damon and J. R. Eshbach, Magnetostatic modes of a ferromagnet slab, J. Phys. Chem. Solids **19**, 308 (1961).

[5] A. F. Franco and P. Landeros, Enhancement of the spin-wave nonreciprocity in antiferromagnetically coupled multilayers with dipolar and interfacial Dzyaloshinskii-Moriya interactions, Phys. Rev. B **102**, 184424 (2020).

[6] K. Szulc, P. Graczyk, M. Mruczkiewicz, G. Gubbiotti, and M. Krawczyk, Spin-Wave Diode and Circulator Based on Unidirectional Coupling, Phys. Rev. Appl. **14**, 034063 (2020).

[7] J. Lan, W. Yu, R. Wu, and J. Xiao, Spin-Wave Diode, Phys. Rev. X **5**, 041049 (2015).

[8] T. Brächer, O. Boulle, G. Gaudin, and P. Pirro, Creation of unidirectional spin-wave emitters by utilizing interfacial Dzyaloshinskii-Moriya interaction, Phys. Rev. B **95**, 064429 (2017).

[9] M. Ishibashi, Y. Shiota, T. Li, S. Funada, T. Moriyama, and T. Ono, Switchable giant nonreciprocal frequency shift of propagating spin waves in synthetic antiferromagnets, Sci. Adv. **6**, eaaz6931 (2020).

[10] O. Gladii, R. Salikhov, O. Hellwig, H. Schultheiss, J. Lindner, and R. A. Gallardo, Spin-wave nonreciprocity at the spin-flop transition region in synthetic antiferromagnets, Phys. Rev. B **107**, 104419 (2023).

[11] P. Bruno and C. Chappert, Oscillatory Coupling Between Ferromagnetic Layers Separated by a Nonmagnetic Metal Spacer, Phys. Rev. Lett. **67**, 1602 (1991).

[12] R. A. Duine, Kyung-Jin Lee, Stuart S. P. Parkin, and M. D. Stiles, Synthetic antiferromagnetic spintronics, Nat. Phys. **14**, 217 (2018).

[13] C. K. Campbell, *Surface Acoustic Wave Devices for Mobile and Wireless Communications* (Academic Press, San Diego, CA, 1998).

[14] D. P. Morgan, *Surface Acoustic Wave Filters: With Applications to Electronic Communications and Signal Processing*, 2nd ed. (Elsevier, Amsterdam, 2007).

[15] S. Mahon, The 5G effect on rf filter technologies, IEEE Trans. Semicond. Manufact. **30**, 494 (2017).

[16] R. M. White and F. W. Voltmer, Direct piezoelectric coupling to surface elastic waves, Appl. Phys. Lett. **7**, 314 (1965).

[17] M. Küß, M. Albrecht, and M. Weiler, Chiral magnetoacoustics, Front. Phys. **10**, 981257 (2022).

[18] P. G. Gowtham, T. Moriyama, D. C. Ralph, and R. A. Buhrman, Traveling surface spin-wave resonance spectroscopy using surface acoustic waves, J. Appl. Phys. **118**, 233910 (2015).

[19] M. Xu, K. Yamamoto, J. Puebla, K. Baumgaertl, B. Rana, K. Miura, H. Takahashi, D. Grundler, S. Maekawa, and Y. Otani, Nonreciprocal surface acoustic wave propagation via magneto-rotation coupling, Sci. Adv. **6**, eabb1724 (2020).

[20] M. Küß, M. Heigl, L. Flacke, A. Hörner, M. Weiler, M. Albrecht, and A. Wixforth, Nonreciprocal Dzyaloshinskii–Moriya Magnetoacoustic Waves, Phys. Rev. Lett. **125**, 217203 (2020).

[21] M. Geilen, A. Nicoloiu, D. Narducci, M. Mohseni, M. Bechberger, M. Ender, F. Ciubotaru, B. Hillebrands, A. Müller, C. Adelmann, and P. Pirro, Fully resonant magneto-elastic spin-wave excitation by surface acoustic waves under conservation of energy and linear momentum, Appl. Phys. Lett. **120**, 242404 (2022).

[22] R. Verba, I. Lisenkov, I. Krivorotov, V. Tiberkevich, and A. Slavin, Nonreciprocal Surface Acoustic Waves in Multilayers with Magnetoelastic and Interfacial Dzyaloshinskii-Moriya Interactions, Phys. Rev. Appl. **9**, 064014 (2018).

[23] M. Küß, M. Heigl, L. Flacke, A. Hörner, M. Weiler, A. Wixforth, and M. Albrecht, Nonreciprocal Magnetoacoustic Waves in Dipolar-Coupled Ferromagnetic Bilayers, Phys. Rev. Appl. **15**, 034060 (2021).

[24] P. J. Shah, D. A. Bas, I. Lisenkov, A. Matyushov, N. X. Sun, and M. R. Page, Giant nonreciprocity of surface acoustic waves enabled by the magnetoelastic interaction, Sci. Adv. **6**, eabc5648 (2020).

[25] R. Verba, V. Tiberkevich, and A. Slavin, Wide-Band Nonreciprocity of Surface Acoustic Waves Induced by Magnetoelastic Coupling with a Synthetic Antiferromagnet, Phys. Rev. Appl. **12**, 054061 (2019).

[26] R. Verba, E. N. Bankowski, T. J. Meitzler, V. Tiberkevich, and A. Slavin, Phase nonreciprocity of microwave–frequency surface acoustic waves in hybrid heterostructures with magnetoelastic coupling, Adv. Electron. Mater. **7**, 2100263 (2021).

[27] H. Matsumoto, T. Kawada, M. Ishibashi, M. Kawaguchi, and M. Hayashi, Large surface acoustic wave nonreciprocity in synthetic antiferromagnets, Appl. Phys. Express **15**, 063003 (2022).

[28] M. Küß, M. Hassan, Y. Kunz, A. Hörner, M. Weiler, and M. Albrecht, Nonreciprocal magnetoacoustic waves in synthetic antiferromagnets with Dzyaloshinskii-Moriya interaction, Phys. Rev. B **107**, 024424 (2023).

[29] V. L. Zhang, K. Di, H. S. Lim, S. C. Ng, M. H. Kuok, J. Yu, J. Yoon, X. Qiu, and H. Yang, In-plane angular dependence of the spin-wave nonreciprocity of an ultrathin film with Dzyaloshinskii-Moriya interaction, Appl. Phys. Lett. **107**, 022402 (2015).

[30] P. J. H. Bloemen, H. W. van Kesteren, H. J. M. Swagten, and W. J. M. de Jonge, Oscillatory interlayer exchange coupling in Co/Ru multilayers and bilayers, Phys. Rev. B **50**, 13505 (1994).

[31] Z. Zhang, L. Zhou, P. E. Wigen, and K. Ounadjela, Angular dependence of ferromagnetic resonance in exchange-coupled Co/Ru/Co trilayer structures, Phys. Rev. B **50**, 6094 (1994).

[32] S. O. Demokritov, Biquadratic interlayer coupling in layered magnetic systems, J. Phys. D **31**, 925 (1998).

[33] G. J. Strijkers, S. M. Zhou, F. Y. Yang, and C. L. Chien, Magnetic characterization and modeling of FeMn/Co/Ru/Co artificial antiferromagnets, Phys. Rev. B **62**, 13896 (2000).

[34] J.-H. Moon, S.-M. Seo, K.-J. Lee, K.-W. Kim, J. Ryu, H.-W. Lee, R. D. McMichael, and M. D. Stiles, Spin-wave propagation in the presence of interfacial Dzyaloshinskii-Moriya interaction, Phys. Rev. B **88**, 184404 (2013).

[35] H. T. Nembach, J. M. Shaw, M. Weiler, E. Jué, and T. J. Silva, Linear relation between Heisenberg exchange and interfacial Dzyaloshinskii–Moriya interaction in metal films, Nat. Phys. **11**, 825 (2015).

[36] M. Weiler, L. Dreher, C. Heeg, H. Huebl, R. Gross, M. S. Brandt, and S. T. B. Goennenwein, Elastically Driven Ferromagnetic Resonance in Nickel Thin Films, Phys. Rev. Lett. **106**, 117601 (2011).

[37] W. P. Robbins, A simple method of approximating surface acoustic wave power densities, IEEE Trans. Son. Ultrason. **24**, 339 (1977).

[38] L. Dreher, M. Weiler, M. Pernpeintner, H. Huebl, R. Gross, M. S. Brandt, and S. T. B. Goennenwein, Surface acoustic wave driven ferromagnetic resonance in nickel thin films: Theory and experiment, Phys. Rev. B **86**, 134415 (2012).

[39] C. Kittel, Interaction of spin waves and ultrasonic waves in ferromagnetic crystals, Phys. Rev. **110**, 836 (1958).

[40] M. Matsuo, J. Ieda, E. Saitoh, and S. Maekawa, Effects of Mechanical Rotation on Spin Currents, Phys. Rev. Lett. **106**, 076601 (2011).

[41] M. Matsuo, J. Ieda, K. Harii, E. Saitoh, and S. Maekawa, Mechanical generation of spin current by spin-rotation coupling, Phys. Rev. B **87**, 180402(R) (2013).

[42] D. Kobayashi, T. Yoshikawa, M. Matsuo, R. Iguchi, S. Maekawa, E. Saitoh, and Y. Nozaki, Spin Current Generation Using a Surface Acoustic Wave Generated via Spin-Rotation Coupling, Phys. Rev. Lett. **119**, 077202 (2017).

[43] Y. Kurimune, M. Matsuo, and Y. Nozaki, Observation of Gyromagnetic Spin Wave Resonance in NiFe Films, Phys. Rev. Lett. **124**, 217205 (2020).

[44] S. Maekawa and M. Tachiki, Surface acoustic attenuation due to surface spin wave in ferro- and antiferromagnets, AIP Conf. Proc. **29**, 542 (1976).

[45] To estimate the approximate amplitude of the induced strain $\varepsilon_{xx,0}$ [58], we assume both IDTs having the same efficiency in SAW excitation and detection. Since the delayline has a total insertion loss of about 92 dB at 6.82 GHz, the loss to excite the SAW in the middle of the delayline is approximately −46 dB. Because the output power of the vector network analyzer is 14 dBm, the power in the middle of the delayline is $P_{\mathrm{SAW}} \approx -32$ dBm. Together with Eq. (3) and the normalized displacement profile $\mathbf{u}(x, z)$ from the FEM simulation of the supplemental material in Ref. [20], we estimate the strain $\varepsilon_{xx,0} \approx 4 \times 10^{-6}$, the magnetoelastic coupling constant $b_1 \approx 4.2$ T, and the maximum magnitude of the acoustic driving field $h_2^l \approx 20\,\mu$T.

[46] K. Ounadjela, A. Arbaoui, A. Herr, R. Poinsot, A. Dinia, D. Muller, and P. Panissod, Interlayer exchange coupling in Co/Ru superlattices, J. Magn. Magn. Mater. **104-107**, 1896 (1992).

[47] S. S. P. Parkin, N. More, and K. P. Roche, Oscillations in exchange coupling and magnetoresistance in metallic superlattice structures: Co/Ru, Co/Cr, and Fe/Cr, Phys. Rev. Lett. **64**, 2304 (1990).

[48] H. Yang, A. Thiaville, S. Rohart, A. Fert, and M. Chshiev, Anatomy of Dzyaloshinskii-Moriya interaction at Co/Pt interfaces, Phys. Rev. Lett. **115**, 267210 (2015).

[49] J. Cho, N.-H. Kim, S. Lee, J.-S. Kim, R. Lavrijsen, A. Solignac, Y. Yin, D.-S. Han, van Hoof, Niels J. J., H. J. M. Swagten, B. Koopmans, and C.-Y. You, Thickness dependence of the interfacial Dzyaloshinskii–Moriya interaction in inversion symmetry broken systems, Nat. Commun. **6**, 7635 (2015).

[50] M. Belmeguenai, J.-P. Adam, Y. Roussigné, S. Eimer, T. Devolder, J.-V. Kim, S. M. Cherif, A. Stashkevich, and A. Thiaville, Interfacial Dzyaloshinskii-Moriya interaction in perpendicularly magnetized $Pt/Co/AlO_x$ ultrathin films measured by Brillouin light spectroscopy, Phys. Rev. B **91**, 180405(R) (2015).

[51] M. Hiebel, *Grundlagen der Vektoriellen Netzwerkanalyse*, 3rd ed. (Rohde & Schwarz, München, 2011).

[52] H. Bouloussa, Y. Roussigné, M. Belmeguenai, A. Stashkevich, S. M. Chérif, J. Yu, and H. Yang, Spin-wave calculations for magnetic stacks with interface Dzyaloshinskii-Moriya interaction, Phys. Rev. B **98**, 024428 (2018).

[53] The propagation velocity of a Rayleigh-type SAW on a pure Y-cut Z-propagation $LiNbO_3$ substrate with a perfectly conducting overlayer of zero thickness is $c_{\mathrm{SAW}} = 3404\,\mathrm{m/s}$ [14]. We assume that c_{SAW} in the real piezoelectric-ferromagnetic heterostructure is slightly lowered [23] because of mass loading and different elastic constants of $LiNbO_3$ and the magnetic films.

[54] G. Bertotti, *Hysteresis in Magnetism: For Physicists, Materials Scientists, and Engineers*, Electromagnetism (Academic Press, New York, 1998).

[55] R. Sasaki, Y. Nii, Y. Iguchi, and Y. Onose, Nonreciprocal propagation of surface acoustic wave in $Ni/LiNbO_3$, Phys. Rev. B **95**, 020407(R) (2017).

[56] We would obtain similar results if we would either assume identical saturation magnetizations $M_s^A = M_s^B$ for our SAF and slightly different thicknesses $d^A < d^B$ or different magnetoelastic constants $b_1^A < b_1^B$.

[57] J. M. Lee, C. Jang, B.-C. Min, S.-W. Lee, K.-J. Lee, and J. Chang, All-electrical measurement of interfacial Dzyaloshinskii-Moriya interaction using collective spin-wave dynamics, Nano Lett. **16**, 62 (2016).

[58] M. Küß, M. Heigl, L. Flacke, A. Hefele, A. Hörner, M. Weiler, M. Albrecht, and A. Wixforth, Symmetry of the Magnetoelastic Interaction of Rayleigh and Shear Horizontal Magnetoacoustic Waves in Nickel Thin Films on $LiTaO_3$, Phys. Rev. Appl. **15**, 034046 (2021).